ACS central science

Research Article

Cite This: ACS Cent. Sci. 2019, 5, 1884−1891

http://pubs.acs.org/journal/acscii

Stretchable and Fully Degradable Semiconductors for Transient Electronics

Helen Tran,[†] Vivian Rachel Feig,[‡] Kathy Liu,[‡] Hung-Chin Wu,[†] Ritchie Chen,[§] Jie Xu,[†,#] Karl Deisseroth,[†,§,∥,⊥] and Zhenan Bao*[,†]

[†]Department of Chemical Engineering, [‡]Department of Material Science and Engineering, [§]Department of Bioengineering, [∥]Department of Psychiatry and Behavioral Sciences, and [⊥]Howard Hughes Medical Institute, Stanford University, Stanford, California 94305, United States

Supporting Information

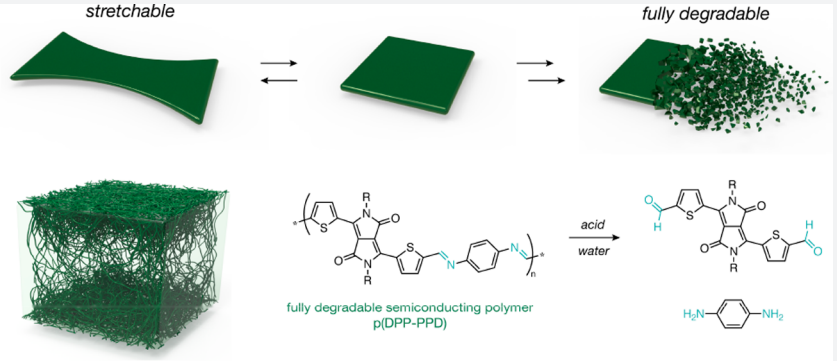

ABSTRACT: The next materials challenge in organic stretchable electronics is the development of a fully degradable semiconductor that maintains stable electrical performance under strain. Herein, we decouple the design of stretchability and transience by harmonizing polymer physics principles and molecular design in order to demonstrate for the first time a material that simultaneously possesses three disparate attributes: semiconductivity, intrinsic stretchability, and full degradability. We show that we can design acid-labile semiconducting polymers to appropriately phase segregate within a biodegradable elastomer, yielding semiconducting nanofibers that concurrently enable controlled transience and strain-independent transistor mobilities. Along with the future development of suitable conductors and device integration advances, we anticipate that these materials could be used to build fully biodegradable diagnostic or therapeutic devices that reside inside the body temporarily, or environmental monitors that are placed in the field and break down when they are no longer needed. This fully degradable semiconductor represents a promising advance toward developing multifunctional materials for skin-inspired electronic devices that can address previously inaccessible challenges and in turn create new technologies.

INTRODUCTION

Electronic devices with skin-inspired properties, particularly stretchability and biodegradability, enable their seamless integration with the natural world, opening doors for remarkable new opportunities for applications in health and environmental monitoring, consumer products, sustainability, and defense.[1−11] For instance, biomedical devices that are stretchable and elastic can intimately conform to organs without eliciting reactive inflammatory responses due to mechanical mismatch, while the ability to degrade eliminates the need for secondary removal surgeries which reduces the likelihood of infection and patient distress.[12−14] The advancement of such electronics critically hinges on the development of biodegradable and stretchable semiconductors to serve as the active component in transistors, a basic element in all modern electronics, ranging from integrated circuits and displays to sensors.

While the fields of transient electronics and stretchable electronics have independently achieved significant milestones in recent years, combining these properties to realize next-generation skin-inspired devices remains an outstanding challenge.[15−19] To date, most reported transient devices use dissolvable thin films of rigid inorganic semiconductors (e.g., silicon nanomembranes) and conductors (e.g., magnesium) as active materials on biodegradable substrates, such as poly(lactic-*co*-glycolic acid) (PLGA).[3,18,20−26] In order to extend the breadth of applications to dynamic systems such as our body, structural engineering-based strategies to impart stretchability on the active materials (i.e., semiconductor and conductor) coupled with the selection of a biodegradable elastomer as the substrate have been employed.[27] Although engineering strategies to impart stretchability to rigid

Received: August 22, 2019
Published: November 13, 2019

DOI: 10.1021/acscentsci.9b00850
ACS Cent. Sci. 2019, 5, 1884−1891

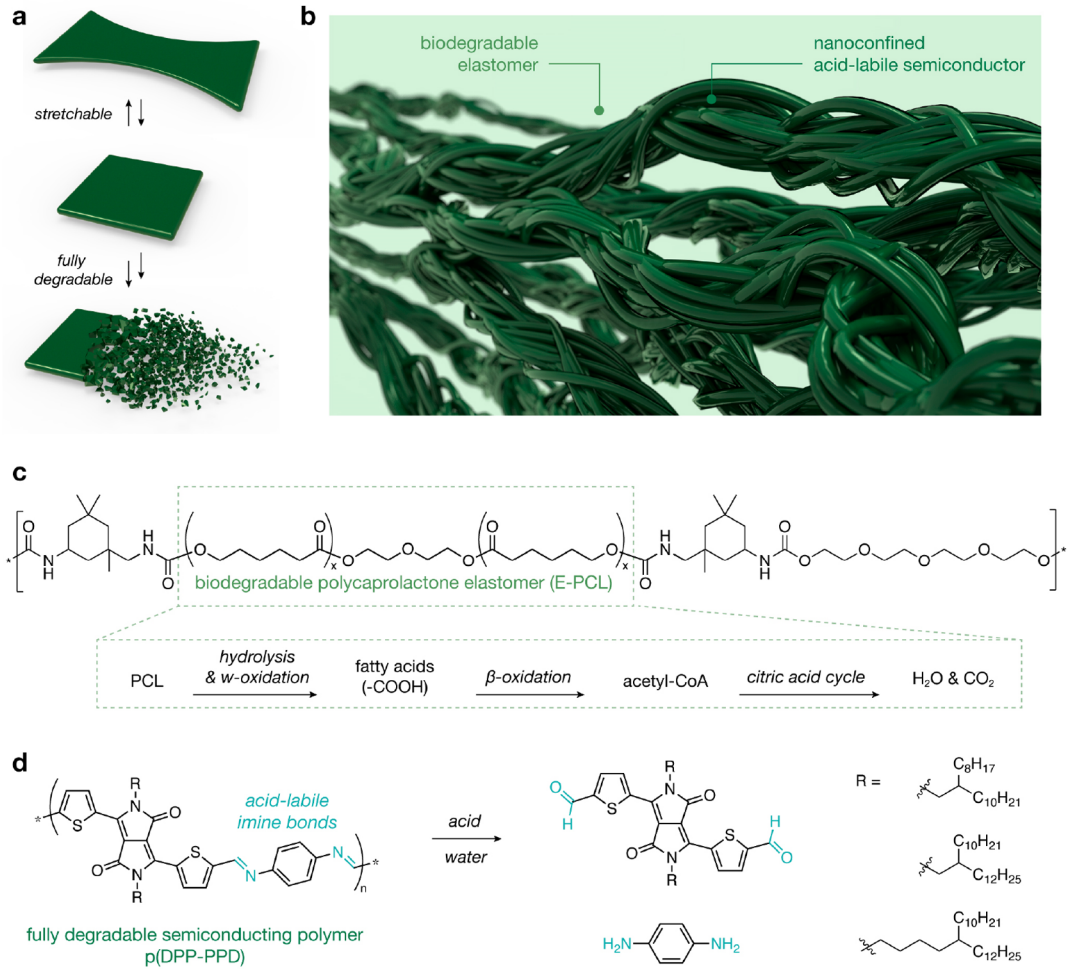

Figure 1. Design of fully degradable semiconducting polymer films through the nanoconfinement effect. (a) Illustration of the dual characteristics, stretchability and full degradability, of the semiconductor designed herein enables its application in transient devices on dynamic surfaces. (b) Illustration of nanoconfined acid-labile semiconductor fibers embedded within a biodegradable elastomer. (c) Chemical structure of the biodegradable elastomer based on polycaprolactone, E-PCL, and the known degradation pathway of PCL. (d) Chemical structure of the fully degradable semiconducting polymer, p(DPP-PPD), and the monomeric byproducts after initial cleavage. Three side-chain designs vary in the alkyl length: $C_1-C_8C_{10}$ (top), $C_1-C_{10}C_{12}$ (middle), and $C_4-C_{10}C_{12}$ (bottom).

inorganic-based semiconductors have led to advances in transient electronics,[27] developing semiconducting polymers that intrinsically possess skin-inspired properties is attractive because of their inherent strain tolerance, scalable fabrication (e.g., minimal device architecture complexity and solution processable), and potential for higher device density.[28]

Compared to inorganic active materials, polymers benefit from a vast chemical design space enabled by synthetic methodologies and are as such a promising class of materials to intrinsically realize the desired combination of stretchability and degradability.[29] Thus, they are easier to modify with additional functionalities downstream (e.g., conformal, self-healing, stimuli-responsive, adhesive) and offer increased control over macroscopic properties like modulus.[30−32] However, imparting both biodegradability and stretchability to semiconducting polymers presents a particular challenge due to the inherent resistance of most charge-conducting chemistries to hydrolytic cleavage and to their typically semicrystalline morphologies.[33] Strategies based on blending or linking an active material with a biodegradable elastomer are realizable, but these materials do not fully degrade to constituent parts.[34,35] Moreover, importantly, the device must operate under strain ideally with identical electrical performance for practical use.

To address this unmet material challenge, we develop a fully degradable, two-component polymeric system that self-assembles into nanoconfined semiconducting fibril aggregates within an elastomeric matrix to enable stretchability (Figure 1a, b and Figures S1−20). Upon nanoconfinement, the increased polymer chain dynamics and suppressed crystallization was found to delay the onset of crack formation under strain.[36,37] Moreover, the deformable interface generated by the elastomeric matrix contributes toward mitigating crack propagation.[36,37] Here, both the matrix and semiconductor are designed to fully degrade into monomeric constituent parts (Figure 1c,d). For the elastomeric matrix, we use a urethane-based polymer (E-PCL) featuring polycaprolactone, a well-established biodegradable material (Figure 1c).[38,39] E-PCL is highly stretchable (over 1000%, Figure 2a) and shows elastic behavior with minor hysteresis over 10 cycles up to 50% strain (Figure 2b and Figure S21). For the semiconductor, we use a diketopyrrolopyrrole-based polymer featuring imine bonds as reversible yet conjugated linkages along the backbone (Figure 1d).[40] The semiconductor is synthesized via stepwise polymer-

DOI: 10.1021/acscentsci.9b00850
ACS Cent. Sci. 2019, 5, 1884−1891

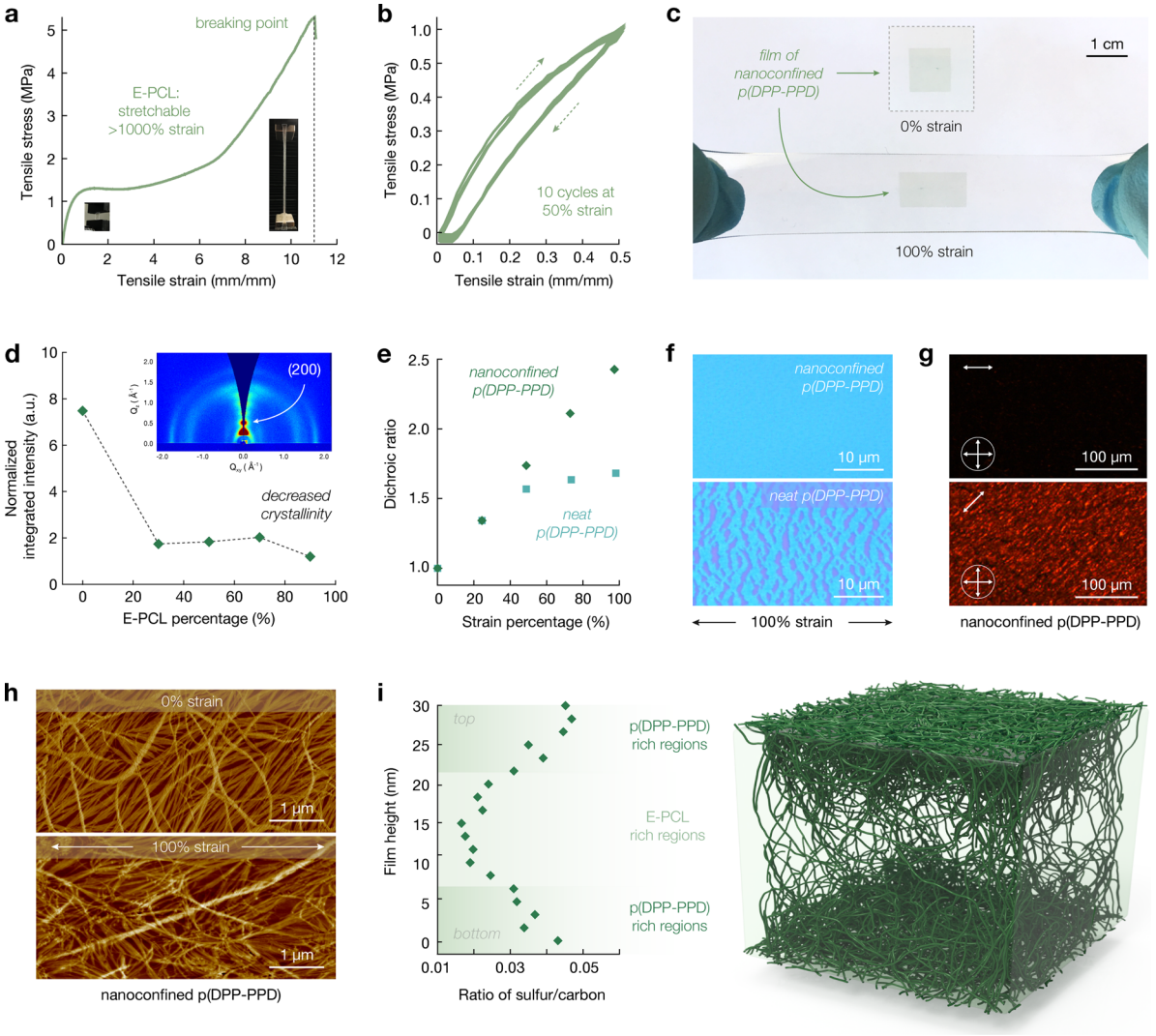

Figure 2. Morphological characterization. (a) Stress−strain curves of E-PCL show stretchability above 1000% strain. Insets show photographs of the elastomer during testing. (b) Ten cycles of stress−strain curves of E-PCL at 30% strain show minor hysteresis upon repeated stretching cycles. (c) Photographs of a film of nanoconfined p(DPP-PPD) transferred to PDMS that was stretched to 100%. (d) Normalized by the semiconductor content, the integrated intensity of the (200) peak extracted from GIWAXS decreases upon nanoconfinement. The inset shows a sample GIWAXS spectra. (e) The change in dichroic ratio upon strain for nanoconfined p(DPP-PPD) is linear, unlike neat p(DPP-PPD), indicating alignment without the formation of thin-film cracks. (f) Bright field images of stretched nanoconfined p(DPP-PPD) strain show a uniform blue thin film, whereas neat p(DPP-PPD) shows cracks. (g) Polarized optical images of nanoconfined p(DPP-DPP) show birefringence along the direction of strain (indicated by top left arrows). (h) Atomic force microscopy images of nanoconfined p(DPP-PPD) at 0% (top) and 100% (bottom) strain. (i) X-ray photoelectron spectroscopy along the depth of the thin film shows a higher sulfur content (sulfur is only present in the semiconductor) at the top and bottom interfaces, as illustrated in the 3D model.

ization of dialdehyde-functionalized DPP and *p*-phenyldiamine [p(DPP-PPD)]. The single-component system of only p(DPP-DPP) is termed "neat p(DPP-PPD)". The blended two-component system of E-PCL and p(DPP-PPD) is termed "nanoconfined p(DPP-PPD)".

RESULTS

Influence of the Side-Chain Design on Nanoscale Phase Segregation. Solubility and the macroscopic aggregation are two preliminary qualitative parameters used for determining whether the side-chain design of p(DPP-PPD) is appropriate to induce proper nanoconfinement, where minimal defects in the films are important to avoid adverse effects on stretchability.[41,42] Defects such as dust particles and precipitated aggregates often localize strain, serving as early points of crack formation. While the imine-based backbone provides degradation, the side chain on the diketopyrrolopyrrole core offers the opportunity to orthogonally tune the solubility. The semiconductor must be sufficiently soluble in the selected solvent, and blended solutions with E-PCL must yield optically homogeneous thin films upon spin coating for consistent device processing.

We first investigate the reported p(DPP-PPD) with C_1−C_8C_{10} branched alkyl side chains as the semiconducting polymer in our nanoconfined system (Figure 1d).[40] Although neat thin films of p(DPP-PPD) with C_1−C_8C_{10} may be prepared, this polymer exhibits insufficiently low solubility (<3 mg/mL in chlorobenzene) and led to precipitates upon solution blending with E-PCL that can be visually observed in

DOI: 10.1021/acscentsci.9b00850
ACS Cent. Sci. 2019, 5, 1884−1891

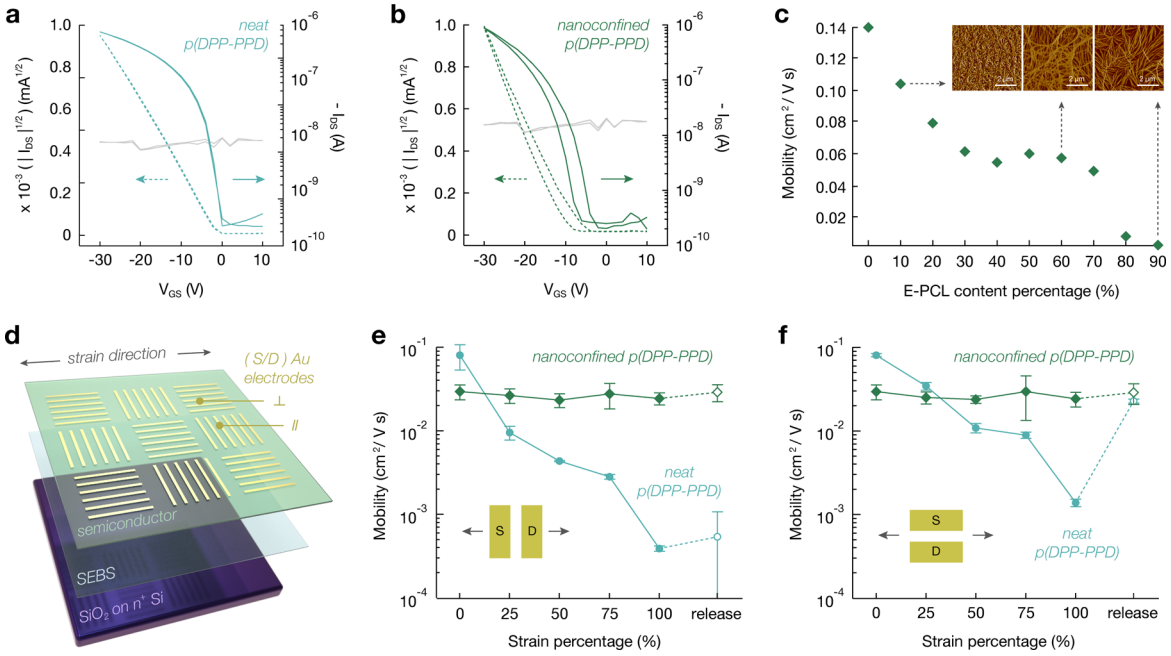

Figure 3. Electrical performance comparison of neat and nanoconfined p(DPP-PDD). (a) A typical transfer curve (V_{DS} = −30 V) of neat p(DPP-PPD) at 0% strain is shown (dashed lines, square root of the drain current; gray lines, I_{GS}). (b) A typical transfer curve (V_{DS} = −30 V) of nanoconfined p(DPP-PPD) at 0% strain is shown (dashed lines, square root of the drain current; gray lines, I_{GS}). (c) The mobility of an FET device of neat and nanoconfined p(DPP-PPD) at different E-PCL content percentages. The insets show AFM images corresponding to 10%, 60%, and 90% E-PCL. (d) Illustration of the device structure for characterizing films under strain feature a layer of SEBS to ensure uniform large-area transfer. (e, f) The change in saturation mobility of neat and nanoconfined p(DPP-PPD) during stretching to 100% strain is shown, both parallel (e) and perpendicular to (f) the charge transport direction.

solution (Figure S22). Thin films of this two-component system were not achieved.

We hypothesize that longer alkyl side chains would increase solubility, leading to the investigation of a second polymer, p(DPP-PPD) with C_1−$C_{10}C_{12}$ branched alkyl side chains (Figure 1d).[43] The alkyl chain with 8 carbons is increased to 12 carbons. Indeed, p(DPP-PPD) with C_1−$C_{10}C_{12}$ is sufficiently soluble in chlorobenzene (3 mg/mL), and nanoscale phase segregation is observed in atomic force microscopy (AFM) images of thin films of blends of 70% E-PCL and 30% p(DPP-PPD) with C_1−$C_{10}C_{12}$ (Figure S23). However, macroscopic aggregation is observed at two length scales in the nanoconfined p(DPP-PPD): (i) an optical image shows micron-sized clusters of p(DPP-PPD) with C_1−$C_{10}C_{12}$ at the top surface of the film, as supported by the X-ray photoelectron spectroscopy (XPS) data (Figures S24−26); (ii) atomic force microscopy (AFM) phase images show micron-sized aggregates of nanofibers that can partially separate upon strain (Figure S23). Aggregates at such length scales limit the degree of interfacing with the soft elastomer and may localize strain at the defects, correspondingly limiting the effectiveness of nanoconfinement as an approach to enhance stretchability.

Thus, we design a third p(DPP-PPD) with C_4−$C_{10}C_{12}$ branched alkyl side chains to further increase solubility and minimize macroscopic aggregation (Figure 1d). Moving the branching position of the side chain away from the backbone has been shown to increase intermolecular interactions by decreasing π−π stacking distances, without compromising solubility.[44] As expected, no micron-sized aggregates were observed on thin films of nanoconfined blends of E-PCL and p(DPP-PPD) with C_4−$C_{10}C_{12}$. Moreover, nanofiber morphologies improve at different blending ratios, as observed in the AFM phase images (Figure S27). For the remainder of this report, all p(DPP-PDD) will refer to polymers with C_4−$C_{10}C_{12}$ branched alkyl side chains.

Investigation of Morphology at the Molecular and Macroscopic Level. Building upon the AFM studies, further insights into the morphology of nanoconfined blends of p(DPP-PPD) and E-PCL are gained through complementary techniques. Grazing-incidence wide-angle X-ray scattering (GIWAXS) shows decreased crystallinity upon nanoconfinement (Figure 2d). Normalized by the semiconductor content, the integrated intensity of the (200) peak shows an approximately 4-fold decrease in crystallinity at different blending ratios. On the basis of previous work and our observation of connected nanofibers in the AFM images, we select 70% E-PCL as an ideal blending ratio for achieving stretchability (Figure 2c and Figure S27).[36] In the thin-film UV−vis absorption spectra, the intensity of the ∼750 nm peak of nanoconfined p(DPP-PPD) is higher than that of the neat p(DPP-PPD), which is indicative of improved packing upon nanoconfinement (Figure S28). As calculated from the ultraviolet−visible (UV−Vis) spectroscopy, the dichroic ratio of a thin film of a nanoconfined blend of 70% E-PCL and 30% p(DPP-PPD) shows a linear increase upon strain, indicative of polymer chain alignment without thin-film crack formation (Figure 2e, f and Figures S29−S31).[45] The thin film of nanoconfined p(DPP-PPD) on 280 nm SiO_2 is optically blue and featureless after 100% strain and transfer (Figure 2f, top). In contrast, the dichroic ratio of the thin film of neat p(DPP-PPD) shows a deviation from the linear trend at strains over 25%, which corresponds to the formation of cracks, which are prominently observed in the bright field images (Figure 2e,f and Figures S29 and S31). The thin film of neat p(DPP-PPD) shows the cracked blue films and underlying purple that corresponds to the 280 nm SiO_2 substrate after 100% strain

DOI: 10.1021/acscentsci.9b00850
ACS Cent. Sci. 2019, 5, 1884−1891

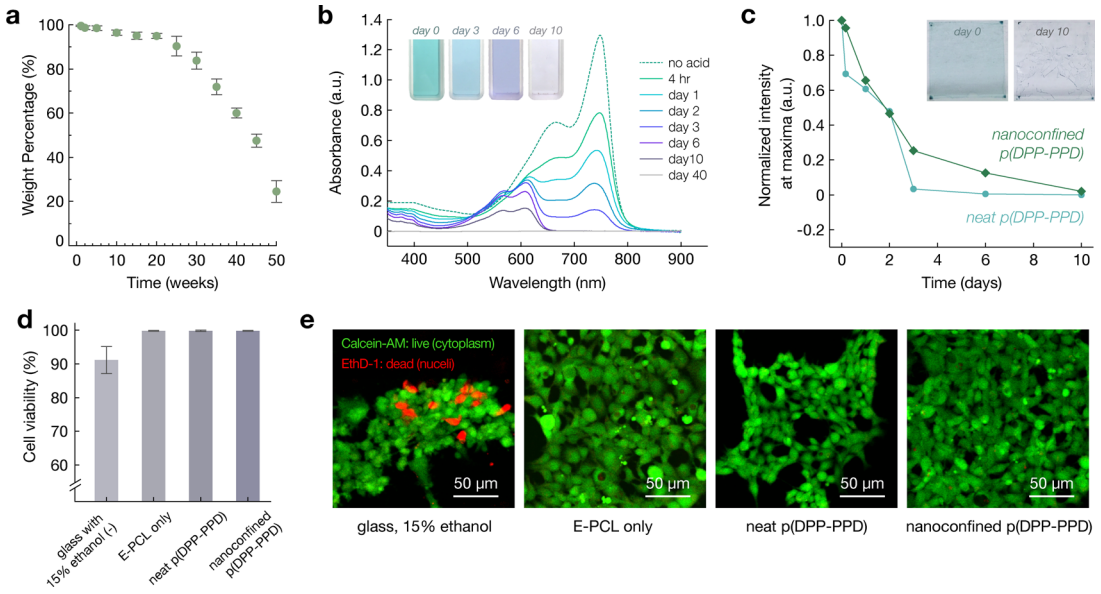

Figure 4. Degradation and biocompatibility characterization of neat and nanoconfined p(DPP-PDD). (a) The weight loss percentage of E-PCL films show degradation with time on the length scale of days. (b) UV−vis absorption spectra of a solution of p(DPP-PPD) in chlorobenzene with the addition of 1% 1 M TFA decreases with time and eventually is negligible by day 40. Inset shows the evolution of color during degradation. (c) The normalized peak maxima extracted from UV−vis absorption spectra of a thin film of neat and nanoconfined p(DPP-PPD) in 1 M TFA water show a gradual decrease with time. The maxima are eventually negligible by day 10. (d) Cell viability for glass with ethanol (negative control), E-PCL, neat p(DPP-PPD), and nanoconfined p(DPP-PPD). (e) Fluorescence images of human embryonic kidney (HEK) 293 cells seeded on the different substrates. The green fluorescence arises from calcein-AM staining of intact cytoplasm. The red fluorescence arises from ethidium homodimer-1 (EthD-1), which is a cell-impermeant nuclear stain. Cells seeded on E-PCL, neat p(DPP-PPD), and nanoconfined p(DPP-PPD) show high cell viability and do not show characteristic red fluorescence indicative of cell death.

and transfer (Figure 2f, bottom). Polarized optical microscopy qualitatively confirms these observations, where birefringence arises when the strain direction is positioned off-angle from both polarizers (Figure 2g and Figure S32). Moreover, the nanofiber alignment upon strain may be directly observed with AFM (Figure 2h). Consistent with our previous findings, in the nanoconfined p(DPP-PPD), AFM phase images and XPS support a model where p(DPP-PPD) nanofibers localize at both the top and bottom interfaces, resulting in an E-PCL rich region at the center of the film (Figure 2i and Figures S33 and S34). GIWAXS shows a slight decrease in lamellar spacing and no change in the $\delta-\delta$ packing upon nanoconfinement, as expected (Figure S35). These morphological characterizations collectively contribute to our hypothesis that blending E-PCL with p(DPP-PPD) leads to the formation of nanoconfined fibers for enhanced stretchability.

Electrical Performance Comparison of Neat and Nanoconfined p(DPP-PPD). Beyond mechanical improvements, we expect that the connectivity between the nanofibril aggregates will enable strain-independent charge transport.[46] First, the electrical performance of neat and nanoconfined p(DPP-PDD) thin films serving as the semiconductor are measured in a thin-film transistor (TFT) with a bottom-gate-top-contact configuration: octadecyltrimethoxysilane (OTS)-modified SiO_2 as the dielectric, highly doped Si as the gate, and Au contacts on the top of the semiconductor as the source and drain (Figure 3a,b and Figures S36 and S37). Notably, the transfer characteristics of nanoconfined p(DPP-PPD) with 70% E-PCL show a slightly suppressed ON current and minor hysteresis that is absent in the transfer characteristics of neat p(DPP-PPD) (Figure 3a,b). We attribute this to presence of polar groups on E-PCL (Figure 1c).[47] This trend is elucidated when comparing the mobility of nanoconfined p(DPP-PPD) at different E-PCL percentage contents, which corresponds to the nanofiber morphologies observed by AFM (Figure 3c). As next-generation imine-based semiconductors are developed, we predict that bottom-gate-bottom-contact configurations will be better suited for the z-phase morphologies observed (Figure 2i).

At 70% E-PCL, there is balance between maintaining a reasonable mobility (~0.05 $cm^2/V{\cdot}s$) and minimizing p(DPP-PPD) content. To investigate the electrical performance of neat and nanoconfined p(DPP-PDD) thin films under strain, we similarly fabricated bottom-gate-top-contact TFTs, but we used a 15 nm interfacial layer of polystyrene-*block*-poly(ethylene-*ran*-butylene)-*block*-polystyrene (SEBS) instead of OTS-functionalization to ensure consistent, large-area transfers (Figure 3d and Figures S38−S40). Although the mobility slightly decreases, this method importantly leads to a more accurate representation of the trend. For both channel directions parallel and perpendicular to strain, the nanoconfined p(DPP-PPD) showed no change in mobility (~0.03 $cm^2/V{\cdot}s$) at strains up to 100% and subsequent release (Figure S41). Minor impact on device performance is achieved through the nanoconfinement of p(DPP-PPD) within E-PCL, which is consistent with the mechanical characterization. In contrast, the neat p(DPP−PPD) showed approximately two orders of magnitude decrease in mobility, consistent with the optical observation of micron-sized cracks (Figure 3e,f and Figure S42).

Degradation Behavior and Biocompatibility. Both components of the nanoconfined p(DPP-PPD) system are designed to degrade in acidic aqueous solutions. We selected 1 M trifluoroacetic acid (TFA, pH ≈ 0.5) in water to accelerate the study time scales. E-PCL degrades slowly, as monitored by weight (Figure 4a). For the semiconductor, the imine bond

DOI: 10.1021/acscentsci.9b00850
ACS Cent. Sci. 2019, 5, 1884−1891

along the backbone hydrolyzes, degrading the polymer into monomeric units, and this process can be monitored in solution as well as thin films of neat and nanoconfined p(DPP-PPD) by UV-Vis spectroscopy.[40] A solution of neat p(DPP-PPD) in 1% 1 M TFA in chlorobenzene shows the gradual absorbance reduction and corresponding solution color change from blue-green to purple to clear (Figure 4b). Similar trends, albeit at slower degradation rates, are observed for thin films of both neat and nanoconfined p(DPP-PPD) in 0.1 M TFA in water (Figure 4c and Figure S43).

Further, the biocompatibility of the materials was investigated to assess its preliminary feasibility for future electronics (Figure 4d). In vitro cell culture experiments of seeding human embryonic kidney (HEK) 293 cells on polymer-coated glass substrates show high viability (>99.5%) on day 2. Cells on E-PCL, neat p(DPP-PPD), and nanoconfined p(DPP-PPD) all show prominent green fluorescence resulting from calcein-AM staining of intact cytoplasm; negligible red fluorescence corresponding to ethidium homodimer-1 (EthD-1), a cell-impermeant nuclear stain indicative of cell death, is observed (Figure 4e). While >99.5% cell viability was observed, cells seeded on neat p(DPP-PPD) films show less cell adhesion and proliferation, which may be attributed to the more hydrophobic nature of the film. This further supports that the nanoconfined p(DPP-PPD), which contains E-PCL, is advantageous.

CONCLUSION

In summary, dual functionality of stretchability and degradability in polymer semiconductors is achieved by harmonizing polymer physics principles of nanoconfinement and molecular design of acid-labile bonds along the polymer backbone. We show that side-chain engineering impacts the formation of nanofibril aggregates, which enables both strain-independent mechanical and electrical properties. This two-component system functions as the first framework to decouple stretchability and degradability in polymer semiconductors. This shift in the design of multifunctional semiconducting polymers away from an all-inclusive, one-component system facilitates the ease of incorporating unexplored skin-inspired functionalities in the future. We expect future advancements in materials and processing to improve device biodegradability and performance. This contributes toward the development of multifunctional, skin-inspired electronics for new technologies in health, sustainability, and information security.

ASSOCIATED CONTENT

Supporting Information

The Supporting Information is available free of charge on the ACS Publications website at DOI: 10.1021/acscentsci.9b00850.

Materials, relevant methods, synthesis and accompanying data; Data include synthetic schemes, NMR, mechanical characterization (stress−strain curves), AFM images, optical microscopy images, XPS depth profile, UV−vis spectra (including for dichroic ratio calculation), polarized optical microscopy images, GIWAXS, output curves, and film thickness determination (by filmetrics and profilometry) (PDF)

AUTHOR INFORMATION

Corresponding Author

*E-mail: zbao@stanford.edu.

ORCID

Helen Tran: 0000-0002-4041-7340
Hung-Chin Wu: 0000-0001-6492-0525
Zhenan Bao: 0000-0002-0972-1715

Present Address

#(J.X.) Nanotechnology and Science Division, Argonne National Laboratory, Lemont, IL 60439, USA.

Author Contributions

H.T. and Z.B. conceived and designed the experiments. H.T. synthesized and characterized all molecules and polymers, completed the mechanical characterizations, fabricated and electrically characterized the transistors, and completed the degradation studies. V.R.F. carried out X-ray photoelectron spectroscopy characterizations and assisted with the mechanical characterizations. K.L. assisted in the NMR collection, device fabrication process, and UV−vis and degradation studies. H.-C.W. completed the GIWAXS characterizations. R.C. completed cell biocompatibility studies. J.X. helped with initial exploratory experiments. H.T. wrote the first draft of the manuscript with contributions from all coauthors.

Notes

The authors declare no competing financial interest.

ACKNOWLEDGMENTS

H.T. was supported by an appointment to the Intelligence Community Postdoctoral Research Fellowship Program at Stanford University, administered by Oak Ridge Institute for Science and Education through an interagency agreement between the U.S. Department of Energy and the Office of the Director of National Intelligence. V.R.F. was supported by the Department of Defense (DoD) through the National Defense Science & Engineering Graduate (NDSEG) Fellowship Program. J.X. acknowledges the Center for Nanoscale Materials, a U.S. Department of Energy Office of Science User Facility, and supported by the U.S. Department of Energy, Office of Science, under Contract No. DE-AC02-06CH11357. K.D. is supported by the Howard Hughes Medical Institute. This work was partly supported by the Air Force Office of Scientific Research (Grant no. FA9550-18-1-0143).

ABBREVIATIONS

PLGA, poly(lactic-*co*-glycolic acid);; PCL, polycaprolactone; DPP, diketopyrrolopyrrole;; PPD, *p*-phenyldiamine; XPS, X-ray photoelectron spectroscopy; AFM, atomic force microscopy; GIWAXS, grazing-incidence wide-angle X-ray scattering; UV−Vis, ultraviolet−visible spectroscopy; OTS, octadecyltrimethoxysilane; SEBS, polystyrene-*block*-poly(ethylene-*ran*-butylene)-*block*-polystyrene; TFA, trifluoroacetic acid; HEK, human embryonic kidney; EthD-1, ethidium homodimer-1

REFERENCES

(1) Someya, T.; Bao, Z.; Malliaras, G. G. The Rise of Plastic Bioelectronics. *Nature* **2016**, *540* (7633), 379−385.

(2) Mimee, M.; Nadeau, P.; Hayward, A.; Carim, S.; Flanagan, S.; Jerger, L.; Collins, J.; McDonnell, S.; Swartwout, R.; Citorik, R. J.; et al. An Ingestible Bacterial-Electronic System to Monitor Gastrointestinal Health. *Science* **2018**, *360* (6391), 915−918.

DOI: 10.1021/acscentsci.9b00850
ACS Cent. Sci. 2019, 5, 1884−1891

(3) Kang, S.-K.; Murphy, R. K. J.; Hwang, S.-W.; Lee, S. M.; Harburg, D. V.; Krueger, N. A.; Shin, J.; Gamble, P.; Cheng, H.; Yu, S.; et al. Bioresorbable Silicon Electronic Sensors for the Brain. *Nature* **2016**, *530* (7588), 71−76.
(4) Chu, B.; Burnett, W.; Chung, J. W.; Bao, Z. Bring on the BodyNET. *Nature* **2017**, *549* (7672), 328.
(5) Barone, D. G.; Malliaras, G. G. Epidermal Electrophysiology at Scale. *Nature Biomedical Engineering* **2019**, *3* (3), 165.
(6) Bettinger, C. J. Advances in Materials and Structures for Ingestible Electromechanical Medical Devices. *Angew. Chem., Int. Ed.* **2018**, *57* (52), 16946−16958.
(7) Chang, J.-K.; Fang, H.; Bower, C. A.; Song, E.; Yu, X.; Rogers, J. A. Materials and Processing Approaches for Foundry-Compatible Transient Electronics. *Proc. Natl. Acad. Sci. U. S. A.* **2017**, *114* (28), E5522−E5529.
(8) Joshipura, I. D.; Finn, M.; Tan, S. T. M.; Dickey, M. D.; Lipomi, D. J. Stretchable Bioelectronics—Current and Future. *MRS Bull.* **2017**, *42* (12), 960−967.
(9) Tian, B.; Liu, J.; Dvir, T.; Jin, L.; Tsui, J. H.; Qing, Q.; Suo, Z.; Langer, R.; Kohane, D. S.; Lieber, C. M. Macroporous Nanowire Nanoelectronic Scaffolds for Synthetic Tissues. *Nat. Mater.* **2012**, *11* (11), 986−994.
(10) Hong, G.; Viveros, R. D.; Zwang, T. J.; Yang, X.; Lieber, C. M. Tissue-like Neural Probes for Understanding and Modulating the Brain. *Biochemistry* **2018**, *57* (27), 3995−4004.
(11) Someya, T.; Amagai, M. Toward a New Generation of Smart Skins. *Nat. Biotechnol.* **2019**, *37* (4), 382.
(12) Boutry, C. M.; Beker, L.; Kaizawa, Y.; Vassos, C.; Tran, H.; Hinckley, A. C.; Pfattner, R.; Niu, S.; Li, J.; Claverie, J.; et al. Biodegradable and Flexible Arterial-Pulse Sensor for the Wireless Monitoring of Blood Flow. *Nature Biomedical Engineering* **2019**, *3* (1), 47.
(13) Cha, G. D.; Kang, D.; Lee, J.; Kim, D.-H. Bioresorbable Electronic Implants: History, Materials, Fabrication, Devices, and Clinical Applications. *Adv. Healthcare Mater.* **2019**, *8* (11), 1801660.
(14) Shin, J.; Liu, Z.; Bai, W.; Liu, Y.; Yan, Y.; Xue, Y.; Kandela, I.; Pezhouh, M.; MacEwan, M. R.; Huang, Y.; et al. Bioresorbable Optical Sensor Systems for Monitoring of Intracranial Pressure and Temperature. *Science Advances* **2019**, *5* (7), No. eaaw1899.
(15) Lipomi, D. J. Stretchable Figures of Merit in Deformable Electronics. *Adv. Mater.* **2016**, *28* (22), 4180−4183.
(16) Li, R.; Wang, L.; Kong, D.; Yin, L. Recent Progress on Biodegradable Materials and Transient Electronics. *Bioactive Materials* **2018**, *3* (3), 322−333.
(17) Tee, B. C.-K.; Chortos, A.; Berndt, A.; Nguyen, A. K.; Tom, A.; McGuire, A.; Lin, Z. C.; Tien, K.; Bae, W.-G.; Wang, H.; et al. A Skin-Inspired Organic Digital Mechanoreceptor. *Science* **2015**, *350* (6258), 313−316.
(18) Kim, H.-S.; Yang, S. M.; Jang, T.-M.; Oh, N.; Kim, H.-S.; Hwang, S.-W. Bioresorbable Silicon Nanomembranes and Iron Catalyst Nanoparticles for Flexible, Transient Electrochemical Dopamine Monitors. *Adv. Healthcare Mater.* **2018**, *7* (24), 1801071.
(19) Shin, J.; Yan, Y.; Bai, W.; Xue, Y.; Gamble, P.; Tian, L.; Kandela, I.; Haney, C. R.; Spees, W.; Lee, Y.; et al. Bioresorbable Pressure Sensors Protected with Thermally Grown Silicon Dioxide for the Monitoring of Chronic Diseases and Healing Processes. *Nature Biomedical Engineering* **2019**, *3* (1), 37.
(20) Hwang, S.-W.; Tao, H.; Kim, D.-H.; Cheng, H.; Song, J.-K.; Rill, E.; Brenckle, M. A.; Panilaitis, B.; Won, S. M.; Kim, Y.-S.; et al. A Physically Transient Form of Silicon Electronics. *Science* **2012**, *337* (6102), 1640−1644.
(21) Koo, J.; MacEwan, M. R.; Kang, S.-K.; Won, S. M.; Stephen, M.; Gamble, P.; Xie, Z.; Yan, Y.; Chen, Y.-Y.; Shin, J.; et al. Wireless Bioresorbable Electronic System Enables Sustained Nonpharmacological Neuroregenerative Therapy. *Nat. Med.* **2018**, *24* (12), 1830−1836.
(22) Yu, K. J.; Kuzum, D.; Hwang, S.-W.; Kim, B. H.; Juul, H.; Kim, N. H.; Won, S. M.; Chiang, K.; Trumpis, M.; Richardson, A. G.; et al. Bioresorbable Silicon Electronics for Transient Spatiotemporal Mapping of Electrical Activity from the Cerebral Cortex. *Nat. Mater.* **2016**, *15* (7), 782−791.
(23) Chiappini, C.; De Rosa, E.; Martinez, J. O.; Liu, X.; Steele, J.; Stevens, M. M.; Tasciotti, E. Biodegradable Silicon Nanoneedles Delivering Nucleic Acids Intracellularly Induce Localized *in Vivo* Neovascularization. *Nat. Mater.* **2015**, *14* (5), 532−539.
(24) Acar, H.; Cınar, S.; Thunga, M.; Kessler, M. R.; Hashemi, N.; Montazami, R. Study of Physically Transient Insulating Materials as a Potential Platform for Transient Electronics and Bioelectronics. *Adv. Funct. Mater.* **2014**, *24* (26), 4135−4143.
(25) Jia, X.; Wang, C.; Zhao, C.; Ge, Y.; Wallace, G. G. Toward Biodegradable Mg−Air Bioelectric Batteries Composed of Silk Fibroin−Polypyrrole Film. *Adv. Funct. Mater.* **2016**, *26* (9), 1454−1462.
(26) Irimia-Vladu, M. Green" Electronics: Biodegradable and Biocompatible Materials and Devices for Sustainable Future. *Chem. Soc. Rev.* **2014**, *43* (2), 588−610.
(27) Hwang, S.-W.; Lee, C. H.; Cheng, H.; Jeong, J.-W.; Kang, S.-K.; Kim, J.-H.; Shin, J.; Yang, J.; Liu, Z.; Ameer, G. A.; et al. Biodegradable Elastomers and Silicon Nanomembranes/Nanoribbons for Stretchable, Transient Electronics, and Biosensors. *Nano Lett.* **2015**, *15* (5), 2801−2808.
(28) Wang, S.; Xu, J.; Wang, W.; Wang, G.-J. N.; Rastak, R.; Molina-Lopez, F.; Chung, J. W.; Niu, S.; Feig, V. R.; Lopez, J.; et al. Skin Electronics from Scalable Fabrication of an Intrinsically Stretchable Transistor Array. *Nature* **2018**, *555* (7694), 83−88.
(29) Kaitz, J. A.; Lee, O. P.; Moore, J. S. Depolymerizable Polymers: Preparation, Applications, and Future Outlook. *MRS Commun.* **2015**, *5* (2), 191−204.
(30) Rogers, J.; Bao, Z.; Lee, T.-W. Wearable Bioelectronics: Opportunities for Chemistry. *Acc. Chem. Res.* **2019**, *52* (3), 521−522.
(31) Tran, H.; Feig, V. R.; Liu, K.; Zheng, Y.; Bao, Z. Polymer Chemistries Underpinning Materials for Skin-Inspired Electronics. *Macromolecules* **2019**, *52* (11), 3965−3974.
(32) Baek, P.; Voorhaar, L.; Barker, D.; Travas-Sejdic, J. Molecular Approach to Conjugated Polymers with Biomimetic Properties. *Acc. Chem. Res.* **2018**, *51* (7), 1581−1589.
(33) Wang, Y.; Ameer, G. A.; Sheppard, B. J.; Langer, R. A Tough Biodegradable Elastomer. *Nat. Biotechnol.* **2002**, *20* (6), 602−606.
(34) Sugiyama, F.; Kleinschmidt, A. T.; Kayser, L. V.; Alkhadra, M. A.; Wan, J. M.-H.; Chiang, A. S.-C.; Rodriquez, D.; Root, S. E.; Savagatrup, S.; Lipomi, D. J. Stretchable and Degradable Semiconducting Block Copolymers. *Macromolecules* **2018**, *51* (15), 5944−5949.
(35) Feig, V. R.; Tran, H.; Bao, Z. Biodegradable Polymeric Materials in Degradable Electronic Devices. *ACS Cent. Sci.* **2018**, *4* (3), 337−348.
(36) Xu, J.; Wang, S.; Wang, G.-J. N.; Zhu, C.; Luo, S.; Jin, L.; Gu, X.; Chen, S.; Feig, V. R.; To, J. W. F.; et al. Highly Stretchable Polymer Semiconductor Films through the Nanoconfinement Effect. *Science* **2017**, *355* (6320), 59−64.
(37) Qian, Z.; Cao, Z.; Galuska, L.; Zhang, S.; Xu, J.; Gu, X. Glass Transition Phenomenon for Conjugated Polymers. *Macromol. Chem. Phys.* **2019**, *220* (11), 1900062.
(38) Middleton, J. C.; Tipton, A. J. Synthetic Biodegradable Polymers as Orthopedic Devices. *Biomaterials* **2000**, *21* (23), 2335−2346.
(39) Heimowska, A.; Morawska, M.; Bocho-Janiszewska, A. Biodegradation of Poly(μ-Caprolactone) in Natural Water Environments. *Pol. J. Chem. Technol.* **2017**, *19* (1), 120−126.
(40) Lei, T.; Guan, M.; Liu, J.; Lin, H.-C.; Pfattner, R.; Shaw, L.; McGuire, A. F.; Huang, T.-C.; Shao, L.; Cheng, K.-T.; et al. Biocompatible and Totally Disintegrable Semiconducting Polymer for Ultrathin and Ultralightweight Transient Electronics. *Proc. Natl. Acad. Sci. U. S. A.* **2017**, *114* (20), 5107−5112.
(41) Mei, J.; Bao, Z. Side Chain Engineering in Solution-Processable Conjugated Polymers. *Chem. Mater.* **2014**, *26* (1), 604−615.
(42) Reid, D. R.; Jackson, N. E.; Bourque, A. J.; Snyder, C. R.; Jones, R. L.; de Pablo, J. J. Aggregation and Solubility of a Model

DOI: 10.1021/acscentsci.9b00850
ACS Cent. Sci. 2019, 5, 1884−1891

Conjugated Donor−Acceptor Polymer. *J. Phys. Chem. Lett.* **2018**, *9* (16), 4802−4807.
(43) Liu, Z.; Zhang, G.; Cai, Z.; Chen, X.; Luo, H.; Li, Y.; Wang, J.; Zhang, D. New Organic Semiconductors with Imide/Amide-Containing Molecular Systems. *Adv. Mater.* **2014**, *26* (40), 6965−6977.
(44) Kang, I.; Yun, H.-J.; Chung, D. S.; Kwon, S.-K.; Kim, Y.-H. Record High Hole Mobility in Polymer Semiconductors via Side-Chain Engineering. *J. Am. Chem. Soc.* **2013**, *135* (40), 14896−14899.
(45) Oh, J. Y.; Rondeau-Gagné, S.; Chiu, Y.-C.; Chortos, A.; Lissel, F.; Wang, G.-J. N.; Schroeder, B. C.; Kurosawa, T.; Lopez, J.; Katsumata, T.; et al. Intrinsically Stretchable and Healable Semiconducting Polymer for Organic Transistors. *Nature* **2016**, *539* (7629), 411−415.
(46) Noriega, R.; Rivnay, J.; Vandewal, K.; Koch, F. P. V.; Stingelin, N.; Smith, P.; Toney, M. F.; Salleo, A. A General Relationship between Disorder, Aggregation and Charge Transport in Conjugated Polymers. *Nat. Mater.* **2013**, *12* (11), 1038−1044.
(47) Lim, S. C.; Kim, S. H.; Koo, J. B.; Lee, J. H.; Ku, C. H.; Yang, Y. S.; Zyung, T. Hysteresis of Pentacene Thin-Film Transistors and Inverters with Cross-Linked Poly(4-Vinylphenol) Gate Dielectrics. *Appl. Phys. Lett.* **2007**, *90* (17), 173512.

DOI: 10.1021/acscentsci.9b00850
ACS Cent. Sci. 2019, 5, 1884−1891